A T3 metering theory used for diesel exhaust fluid dosing and failure diagnosis in selective catalyst reduction dosing systems

Yan-xiang YANG[1], Bing-qian TAN[†‡2], Chang-wen LIU[2], Ping ZHANG[3], Qi-jiang LE[3], Ben-xi ZHANG[4]

[1]Institute of Internal Combustion Engines, Tianjin University, Tianjin 300072, China

[2]State Key Laboratory of Engines, Tianjin University, Tianjin 300073, China

[3]Zhejiang FAI Electronics Co., Ltd, Hangzhou 310018, China

[4]Department of Energy Engineering, Zhejiang University, Hangzhou 310027, China

[†]E-mail: tanbingqian@tju.edu.cn

Received Sept. 11, 2018; Revision accepted Mar. 17, 2019; Crosschecked Mar. 19, 2019

Abstract: In this paper, a new dosing unit is presented for diesel exhaust fluid (DEF) dosing in combustion engine exhaust emission selective catalyst reduction (SCR) systems. The dosing unit is a plunger-sleeve pump nozzle system driven by a charged solenoid, and is pump-end controlled by pulse width modulation (PWM) signals. The core characteristics of the unit include both metering precision control and failure diagnosis methods. In this study, both physical-mathematical analysis and experiments were carried out. A so-called whole state T3 metering theory was developed by studying the system using a physical-mathematical model based on energy conservation. The study showed that the liquid discharge, which is associated with the plunger-sleeve relative position, correlates well with a measurable variable T3. Experimental investigations verified that the metering results were independent of the state variations in some range and that metering is controlled with high precision. Two typical DEF dosing systems based on the dosing unit and some specific failure modes are introduced. Significant variation of the parameter T_3 in the T3 model is useful for the detection of specific failure modes.

Key words: Diesel exhaust fluid (DEF) dosing unit; Plunger-sleeve pump; T3 metering theory; Sensor-free diagnosis

https://doi.org/10.1631/jzus.A1800518   **CLC number:** TK421.5

1 Introduction

Due to the continuous deterioration of global environments, stricter regulations aimed at reducing internal combustion (IC) engine emissions have been issued and implemented by many governments (David, 1998). In Europe, the Euro VI Standard has been implemented since 2013. In China, the China V Standard was implemented for heavy duty diesel engines in 2017, and the China VI Standard was is-

sued and is to be implemented in July, 2019. For diesel engines, NO_x is one of the main pollution emissions (Patel and Patel, 2012). For heavy duty diesel engines, the China VI Standard limits NO_x emissions to 0.4 g/(kW·h), which is much lower than the limit of 2 g/(kW·h) in China V. In addition, even stricter regulations will be issued and implemented in the next few years.

Some researchers have concluded that the largest reduction in emissions achievable by combustion process improvement and strategy optimization can meet only the Euro IV Standard (Koebel and Kleemann, 2000; Oh and Lee, 2014). Based on the mechanical structure and combustion organization method of existing diesel engines, with some aftertreatment processes, such as exhaust gas recirculation

(EGR) and selective catalytic reduction (SCR), the reduction of NO_x emissions needed to meet the stricter regulations can be achieved (Grout et al., 2013). The SCR system has a wide effective temperature window and high NO_x reduction efficiency (Fedeyko et al., 2009; Brandenberger et al., 2010). For diesel engines, large decreases in particulate emissions and fuel consumption can be achieved by using the trade-off curve feature (Scarnegie et al., 2003; Lambert et al., 2004; Cloudt et al., 2009; Heeb et al., 2011), while increased NO_x emissions can be eliminated with an SCR system. At present, the diesel exhaust fluid (DEF) most often used in SCR systems is an aqueous mixture of urea and water, with a urea concentration of 32.5% (Moreno-Tost et al., 2008; Biswas et al., 2009; Hamada and Haneda, 2012).

The dosing unit plays a very important role in an SCR system. DEF is dosed and atomized when supplied to the exhaust stream by a dosing unit, which follows the dosing rate command given by a dosing control unit (DCU). Both the dosing rate and distribution play important roles in ammonia availability and distribution in the exhaust pipe before the ammonia arrives at the catalyst, thus affecting the NO_x reduction efficiency. A shortage of DEF will lead to a decrease in reduction efficiency, while an overdose results in too much ammonia slip (Wang et al., 2008), which also has a negative impact on the environment.

Dosing and injection in IC engines are usually carried out by a pump-nozzle system. Existing SCR dosing pumps, whether air-assisted or airless type, mostly use diaphragm pumps. In typical air-assisted type diaphragm pumps, liquid discharged in each cycle is dosed by constant volume metering, and the dosing rate is then controlled by positive pump revolution counting. In typical airless type diaphragm pumps, the pumps are used to supply DEF and maintain a stable liquid pressure in the pipe connecting the pump and nozzle. Metering is then controlled by nozzle-open time. The dosing systems with both diaphragm pumps are usually complicated and have difficulties in deicing and anti-clogging.

A dosing unit designed for DEF by Delphi (Lee et al., 2010; Needham et al., 2012) (Fig. 1), uses an operating principle which is different from that of the pump-nozzle system. It is a linear plunger pump driven by electro-magnetic force from a solenoid coil. This type of plunger pump was invented by Ficht

(Heimberg et al., 1996) and is now widely used in IC engines, especially for gasoline injection.
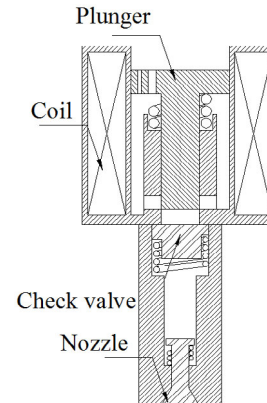

Fig. 1 A type of plunger pump

Different from the plunger pump, Fig. 2 shows an innovative design of a dosing unit called a sleeve pump, made by Zhejiang FAI Electronics Co., Ltd (FAI in short) in China. Its distinguishing feature is that the liquid is delivered by a type of sleeve with a free armature rather than a plunger motion, and the armature is free of the ball valve 1.

When the solenoid coil is energized at $t=0$ with a pulse width of t_1, the current in the coil first grows, then in some cases drops a little, and rises again after a period of time (Fig. 3). Once the coil is de-energized at $t=t_1$, an induced voltage is generated and the current reaches its maximum i_1 and then drops rapidly to zero.

During this process, the sleeve is driven by the magnetic force, and at first moves downward. As the sleeve moves, it closes the ball valve 1 and the continuous movement enlarges the pressure in the chamber between ball valves 1 and 2. The high pressure liquid goes through the ball valve 2 and injection occurs. The sleeve then returns to its original position a period of time after the current drops to zero.

In the above process, a number of parameters relating time and position are involved. For a given power level, the minimum pulse width resulting in mass discharge onsets is defined as the drop-out pulse width. The drop-out pulse width is almost equal to t_{1d}, the time at which the current passing through the coil stops growing. The maximum current for a given power pulse is equal to i_1, which is here defined as

end-up current. The maximum displacement which the armature can travel for a given power pulse is denoted by x_e, and the time taken is denoted by t_e. The end-up current corresponding to the drop-out pulse width is defined as the drop-out current i_d. The maximum displacement which the armature can travel under the drop-out pulse width is defined as the drop-out displacement, denoted by x_d.
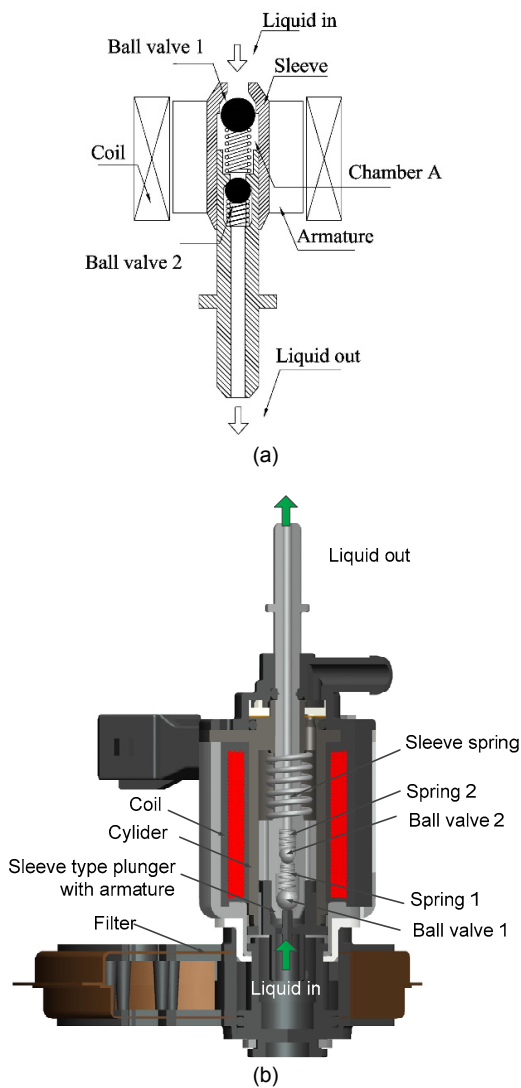

(a)

(b)

Fig. 2 Sleeve pump
(a) Physical model; (b) Detailed structure

However, the dosing rate is no longer proportional to the input pulse width. The theoretical model predicting the liquid discharge rate for a sleeve pump type dosing unit is far more sophisticated than that for a conventional injection system with a fuel rail

(Heywood, 1988). The dosing units of FAI and Delphi are similar, and can be referred to as plunger-sleeve pump-nozzle systems. This kind of dosing unit can be considered an electro-mechanical system, consisting of an electro-mechanical energy conversion part and a working part. Because the unit is propelled by pulse width modulation (PWM) power from a DCU (Fig. 4), the liquid dosing device is a pump-end controlled pump-nozzle dosing unit. The coil is untouched by the dosing liquid, thereby avoiding infection of the conducting liquid. The complexity and weight of the unit are far lower than that of traditional dosing pumps. Similar designs are available in the latest patents of Bosch (Matthias, 2015).
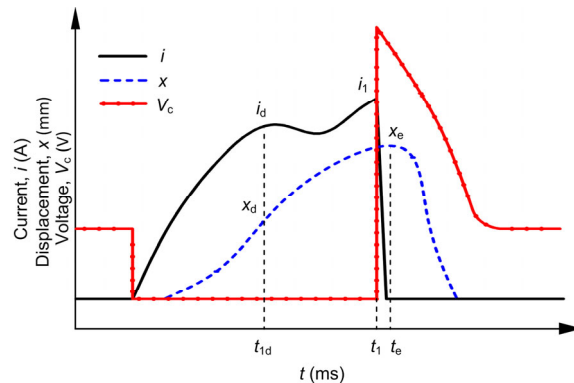

Fig. 3 Variation in the current passing through the coil wire in an FAI sleeve pump

Fig. 4 shows a physical model of the pump. E is the power source voltage, λ is the flux linkage, x is the displacement of the plunger with an initial value of x_0, and f_{fld} is the electric filed force. The operation of the system is related to several different forces, including a spring force characterized by the spring coefficient K, a pressure force f_p producing a network for liquid delivery, a damper force characterized by the damper constant D opposing the armature motion, and an inertia force characterized by the total mass M of the moving parts. The sum of the four kinds of forces is equal to the electric field force provided by the energy conversion part. Like the sleeve pump, the plunger pump as a Delphi pump shares the same physical model.

Compared with the traditional magnetic injector of Bosch, the difficulty of such an electro-mechanical

energy conversion system in controlling the liquid delivery rate lies in that the output of the system is inherently subject to variation due to state changes. A change of state could be caused by:

1. A change in the electric resistance of the wire;
2. A change in the viscosity of the liquid;
3. A change in the phase of the liquid in the armature chamber (Kim and Richardson, 1995);
4. Fluctuation in power levels (supply voltage);
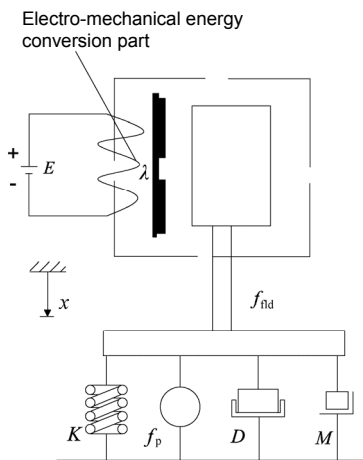5. Mechanical wear of moving parts.

Fig. 4 Physical model of a sleeve pump

In actual SCR system applications, some problems will affect the precision of metering. First, the voltage of the battery is not stable. The temperature in the solenoid coil increases as a result of the long operating time. This increases the resistance of the wire, which causes a reduction in the current in the coil. A state change of temperature always leads to a decrease in the viscosity of a liquid, and some gas will separate from the liquid. Due to the sophisticated determination of the discharge rate, high metering precision cannot be achieved by direct adjustment of driving pulse width T_1. Therefore, a theoretical investigation of the liquid metering model, free from the state variation in some range, is fairly significant for a plunger-sleeve pump.

On the other hand, for SCR system applications, failure modes of plunger-sleeve pumps, which cause a reduction in NO_x conversion efficiency or even loss of function, are stipulated to be detectable by the requirement of on-board diagnosis (OBD) regulations. Various sensors are used for failure detection, but sensors add cost and lead to higher failure rates for the whole dosing system. If the results of our theoretical investigation also have instructional significance for failure mode detection, the plunger-sleeve pump and its control method will have more advantages.

In the following sections, a new parameter T3 is proposed from investigation of the physical process of a plunger-sleeve pump type dosing unit. The new parameter measures the close linkage among the energy balance, liquid discharge, and other relevant electric variables. The study reveals that an electrically characterized parameter T3 is associated with the net output energy, and results directly in liquid discharge. The finding and definition of the dimensionless parameter T3 lay the foundation for a whole-state fuel measurement model, free from state variation. Intensive experiments have been carried out to verify the theory. Furthermore, the flexible usage of T3 is proved to be reliable for detecting some typical failure modes of plunger-sleeve pumps.

2 Theory descriptions

The system shown in Fig. 4 can be described mathematically in terms of an energy conservation equation and an electric equation (Fitzgerald et al., 2003). The equations vary with the difference in driving circuitry. A typical electric circuit used for driving the electro-mechanical system is shown in Fig. 5. A metal-oxide semiconductor field-effect transistor (MOSFET) switch is employed to produce the PWM power, R is a resistor for protecting the electric switch, and r is the electric resistance in the coil wire.

2.1 Governing equations

For the electro-mechanical energy conversion system in a plunger-sleeve pump, both energy conservation and electric circuit principles are employed in setting up the governing equations. The total energy output of the electromagnetic system within the time increment of dt, $(ei-ri^2)dt$, is dispensed by the following items: $K(x+x_0)dx$ is the work done by the spring force; $f_p dx$ is the mechanical energy output by the plunger; $D\dfrac{dx}{dt}dx$ is the work done by the damper force, and w_{fld} is void electric field energy stored in the system. i is the electric current in the coil, and e is the power source voltage.

The energy balance equation is given by

$$\int_0^{t_1}(ei-ri^2)\mathrm{d}t=\int_0^{x_e}D\frac{\mathrm{d}x}{\mathrm{d}t}\mathrm{d}x+\int_0^{x_e}K(x+x_0)\mathrm{d}x \\ +\int_{x_d}^{x_e}f_p\mathrm{d}x+w_{\mathrm{fld}}. \tag{1}$$

According to Fig. 5, the electric equations are given by

$$\frac{\mathrm{d}\lambda}{\mathrm{d}t}=e-ir, \quad t\le t_1, \tag{2}$$

$$\frac{\mathrm{d}\lambda}{\mathrm{d}t}=e-iR, \quad t>t_1. \tag{3}$$

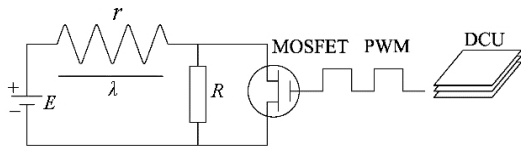Both the energy equation and the electric equations are also applicable to plunger pumps.

Fig. 5 A typical driving circuitry

It is difficult to obtain an analytical solution from the above three equations. The pressure force f_p and the damper constant D are unknown, and the governing equations are too complicated to be solved by a microprocessor during the process of engine operation. Consequently, simplifications of the energy balance Eq. (1) have to be made in practice. One of the simplifications widely used for plunger pumps as Delphi pumps is that only the current integral term on the left side of Eq. (1) is considered, which is supposed to be proportional to the fuel discharge rate in a sleeve pump (Hayakawa, 2007).

The energy balance Eq. (1) can be rewritten in dimensionless form as

$$\int_0^{T_1}(EI-\bar{r}I^2)\mathrm{d}\tau=\int_0^{X_e}\bar{D}\frac{\mathrm{d}X}{\mathrm{d}\tau}\mathrm{d}X \\ +\int_0^{X_e}\bar{K}(X+X_0)\mathrm{d}X+\int_1^{X_e}F_p\mathrm{d}X+W_{\mathrm{fld}}. \tag{4}$$

The dimensionless electric Eqs. (2) and (3) are

$$\frac{\mathrm{d}\Lambda}{\mathrm{d}\tau}=E-\bar{r}I, \quad \tau<T_1, \tag{5}$$

$$\frac{\mathrm{d}\Lambda}{\mathrm{d}\tau}=E-I\bar{R}, \quad \tau>T_1. \tag{6}$$

The scales for the nondimensionalized parameters are listed below.

A. Time: $t_{1\mathrm{d}}$, the drop-out pulse width.

B. Length: x_{d}, the drop-out displacement.

C. Mass: Q_0, the maximum mass discharge of the liquid.

D. Reference voltage, v_{ref}.

The dimensionless variables and parameters are defined by the equations shown in Table 1.

Table 1 Dimensionless parameter transformation

No.	Transformation
(a)	$\tau=t/t_{1\mathrm{d}}$
(b)	$X=x/x_{\mathrm{d}}$
(c)	$T_1=t_1/t_{1\mathrm{d}}$
(d)	$X_{\mathrm{e}}=x_{\mathrm{e}}/x_{\mathrm{d}}$
(e)	$X_0=x_0/x_{\mathrm{d}}$
(f)	$F_{\mathrm{p}}=f_{\mathrm{p}}\big/(Q_0x_{\mathrm{d}}/t_{1\mathrm{d}}^2)$
(g)	$W_{\mathrm{fld}}=w_{\mathrm{fld}}\big/(Q_0x_{\mathrm{d}}^2/t_{1\mathrm{d}}^2)$
(h)	$E=e/v_{\mathrm{ref}}$
(i)	$I=i\big/\big[Q_0x_{\mathrm{d}}^2/(t_{1\mathrm{d}}^3v_{\mathrm{ref}})\big]$
(j)	$\Lambda=\lambda/(v_{\mathrm{ref}}t_{1\mathrm{d}})$
(k)	$\bar{r}=r\big/\big[v_{\mathrm{ref}}^2t_{1\mathrm{d}}^3/(Q_0x_{\mathrm{d}})\big]$
(l)	$\bar{R}=R\big/\big[v_{\mathrm{ref}}^2t_{1\mathrm{d}}^3/(Q_0x_{\mathrm{d}})\big]$
(m)	$\bar{D}=D/(Q_0/t_{1\mathrm{d}}^3)$
(n)	$\bar{K}=K/(Q_0/t_{1\mathrm{d}}^2)$

2.2 Pressure model

The discharge amount Q is associated with the mechanical energy W_{p} output by the sleeve type plunger, which is the part of $\int_1^{X_e}F_{\mathrm{p}}\mathrm{d}X$ in Eq. (4).

But a pressure model needs to be proposed first before the relationship of Q and W_{p} can be defined.

The pressure P in the chamber A between ball valves 1 and 2 (Fig. 2) can be expressed as

$$P=\sum_{j=0}^{n}\beta_j(X_{\mathrm{e}})X^j, \quad 1<X<X_{\mathrm{e}}, \tag{7}$$

where P satisfies the following boundary conditions:

$$P(X=1) = P(X=X_e) = P_0, \qquad (8)$$

$$\frac{\partial}{\partial X_e}\left(\frac{\partial^{n-1}P}{\partial X^{n-1}}\right)\Bigg|_{X=1} = 0, \qquad (9)$$

where P_0 is the open pressure of ball valve 2, which is designed in a specific dosing unit.

By substituting Eq. (7) into Eqs. (8) and (9), a second-order approach to P can be expressed as

$$P = \frac{\Omega}{X_e - 1}(X-1)(X_e - X) + P_0, \qquad (10)$$

where Ω is a constant and can be determined by the following relation:

$$\Omega = \frac{4P_{max}}{X_e - 1}, \qquad (11)$$

where the dimensionless parameter P_{max} is a measureable constant representing the maximum pressure in the chamber A.

2.3 Q-W_p relation

As discussed above, W_p can be derived as

$$W_p = \int_1^{X_e} F_p dX = A_p\left[\frac{\Omega}{6}(X_e - 1)^2 + P_0(X_e - 1)\right], \qquad (12)$$

where A_p is the cross-section area of the chamber A.

By substituting the dimensionless volume displacement $\Delta V = A_p(X_e - 1)$ into Eq. (12), we have

$$W_p = \frac{\Omega}{6A_p}\Delta V^2 + P_0\Delta V. \qquad (13)$$

The volume displacement ΔV consists of two parts: the volume discharge of the liquid passing through the ball valve 2, ΔV_i, and the leakage through the tolerance of the sleeve type plunger, ΔV_l. The ratio of the volume displacement to the volume discharge through the ball valve 2 can be defined as the charging coefficient $\eta(Q)$, expressed as

$$\eta(Q) = 1 + \frac{\Delta V_l}{\Delta V_i}. \qquad (14)$$

The relation between the volume displacement and the mass discharge is therefore given by

$$\Delta V = \frac{Q}{\Pi}\eta(Q), \qquad (15)$$

where Π is the dimensionless density of the fuel.

By substituting Eq. (15) into Eq. (13), we have

$$Q^2 + \frac{6A_p\Pi P_0}{\Omega\eta(Q)}Q = \frac{6A_p\Pi^2}{\Omega\eta^2(Q)}W_p. \qquad (16)$$

The charging coefficient $\eta(Q)$ is a function of Q, given in Eq. (17), which is a designed parameter that can be controlled in production.

$$\eta(Q) = Q^n. \qquad (17)$$

3 T3 theory

3.1 Definition of T_3

Once the solenoid coil is de-energized by switching off the MOSFET, the circuit is controlled by Eq. (6). Integrating both sides of Eq. (6) in the interval of (T_1, T_e), we have

$$\Lambda_1 = \int_{T_1}^{T_e} V_r d\tau, \qquad (18)$$

where $V_r = \bar{I}R - E$ is the dimensionless electric potential relative to the ground at the place between the coil and the MOSFET switch, and Λ_1 is the dimensionless flux linkage at $\tau = T_1$.

According to the mean value theorem of integrals, Eq. (18) can be simplified as

$$\Lambda_1 = V_r(\xi)(T_e - T_1), \qquad T_1 < \xi < T_e. \qquad (19)$$

A typical variation in the voltage V_r with time is shown in Fig. 6, in which the right side of Eq. (19) is represented by the shaded area *a-b-c*. To measure

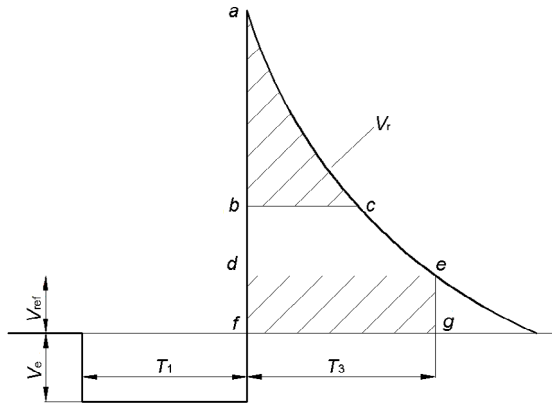the shaded area *a-b-c*, the following approach is proposed.

Fig. 6 V_r time history

The time duration is defined as T_3, within which the induction voltage V_r decays from its maximum value to a reference voltage V_{ref}. It is chosen in such a way that the area of the shaded area *a-b-c* is approximately proportional to the area *d-e-f-g* for various T_1, that is

$$\Lambda_1 = V_e(\xi)(T_e - T_1) = CT_3, \qquad T_1 < \xi < T_e, \qquad (20)$$

where $C>0$ is a dimensionless constant. The variables T_3 and V_r are shown in Fig. 6.

After the electric Eq. (5) is timed by current *I*, integrating both sides of the equation within the interval of (0, T_1) gives

$$\int_0^{T_1} I \frac{d\Lambda}{d\tau} d\tau = \int_0^{T_1} (EI - \bar{r}I^2) d\tau. \qquad (21)$$

The left side of Eq. (21) can be expressed as the sum of two integrals:

$$\int_0^{T_1} I \frac{d\Lambda}{d\tau} d\tau = \int_0^1 I \frac{d\Lambda}{d\tau} d\tau + \int_1^{T_1} I \frac{d\Lambda}{d\tau} d\tau. \qquad (22)$$

As discussed above, the current *I* in the interval of (1, T_1) is basically invariant, and is approximately equal to I_1. By substituting Eqs. (20)–(22) into Eq. (4), the mechanical energy output by the sleeve-plunger pump can be derived as

$$W_p = \int_0^{\Lambda_1} I d\Lambda - I_1\Lambda_d + CI_1T_3 - W_{fld}$$
$$- \int_0^{X_e} \bar{D} \frac{dX}{d\tau} dX - \bar{K}X_e \left(\frac{X_e}{2} + X_0 \right), \qquad (23)$$

where Λ_d indicates Λ when $T=T_{1d}$. For a specific dosing unit, the part $\int_0^{\Lambda_1} I d\Lambda - I_1\Lambda_d$ is a constant, based on the above discussion. The total energy output therefore varies with T_3.

3.2 Whole-state model of liquid measurement

A mass discharge equation in term of T3 can be derived by substituting Eqs. (4) and (23) into Eq. (16), as follows:

$$Q^2 + \alpha Q = \beta I_1 T3, \qquad (24)$$

where

$$\alpha = \frac{6A_p \Pi P_0}{\Omega \eta(Q)}, \qquad (25)$$

$$\beta = \frac{6A_p C\Pi^2}{\Omega \eta^2(Q)}, \qquad (26)$$

$$T3 = T_3 - T_{3b}, \qquad (27)$$

$$T_{3b} = \left[I_1\Lambda_d - \int_0^{\Lambda_1} I d\Lambda + W_{fld} + \int_0^{X_e} \bar{D} \frac{dX}{d\tau} dX \right.$$
$$\left. + \bar{K}X_e \left(\frac{X_e}{2} + X_0 \right) \right] \bigg/ (CI_1). \qquad (28)$$

Eq. (24) is here referred to as the whole-state model for liquid dosing. It describes the relation of mass discharge *Q* to end-up current I_1 and variable T3, which is free from state variation.

In both α and β, the parameters are state independent, so these two coefficients are state independent. I_1 has little influence on the mass discharge rate compared with variable T3. Therefore, it is better to treat I_1 as a state-related parameter rather than a variable.

The reason that Eq. (24) is free from state variation is that parameter T_{3b} takes all of the state variation-related factors from variable T_3. As defined in Eq. (27), T_{3b} contains all of the state variation-related items.

3.3 Determination of T_{3b}

T_{3b} is defined as a time parameter. As shown in Eq. (24), it consists of various state-related parameters

and always influences the effective energy of the electro-magnetic part. Fortunately, the effects can be reduced or even eliminated by pre-calibration in practical application.

Considering that T_{3b} is a function of T_1, T_{3b} can be expanded by T_1 as a Taylor series expansion. When the precision requirement and calculating speed are taken into account, a second-order form is given as

$$T_{3b} = \alpha_1 T_1^2 + \alpha_2 T_1 + \alpha_3. \qquad (29)$$

To calibrate T_{3b}, a series of data of T_1-measured Q and T_3 is matched, and the values of α_1, α_2, and α_3, then α and β are determined. Then, the stable relation between Q and T3 is achieved.

Although T_{3b} contains a couple of state-related items, not all of them can be matched in T_{3b}. Only those largely affecting the discharge rate and which are measurable are taken into account, for example, power source voltage. Temperature is also one of the main factors affecting metering precision, but it is difficult to measure in practice. Experimental results have shown its direct and obvious influence on T_3. Based on these results, a dynamic calibration is used to fix the effect in application. The strategy involves driving the dosing unit periodically with a short power pulse T_1, which is not long enough to form injection, and recording the corresponding T_3 as an indicator of temporal state variation. The difference between T_3 and T_{3b} manifests the state changes caused by the temperature, and relevant adjustment of T_1 will be made.

The above methods can make T3 be close to the theoretical T3, which keeps the T3-Q relation stable under the main effects resulting from the main state changes.

4 Verification of T3 theory

To validate T3 theory, a weighing method was used to test the relations T_1-Q and T3-Q. During each test, the test cycle was set to 1000, and the operating frequency to 60 Hz.

The mass discharge Q under a specific T_1 increases with increasing power source voltage (Fig. 7). This reveals the obvious influence of power source

voltage on metering precision. T_3 values and initial T_3 values (T_{30}) were recorded at the beginning of the tests, parameter values of α_1, α_2, and α_3 were calculated by fitting under different power levels, and T_{3b} was obtained (Fig. 8). The re-plotted relations of T3-Q are shown in Fig. 9. The dispersed data points at different voltages fit onto one line.
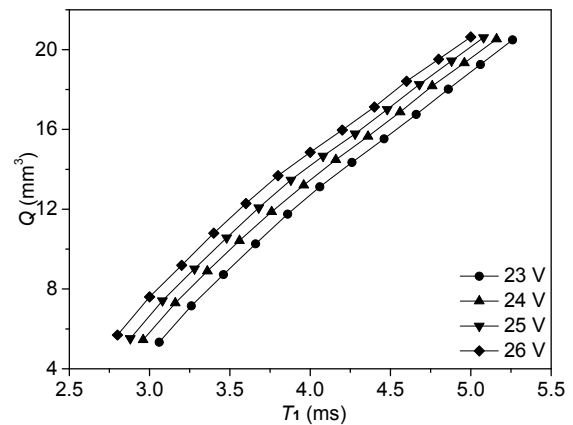

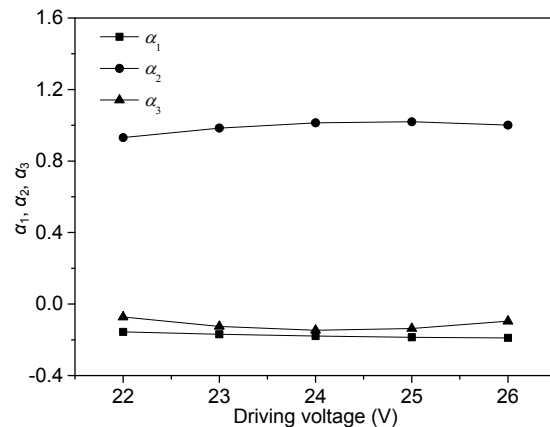**Fig. 7 Mass discharge variation caused by changes in the power level**

Fig. 8 Variation in T_{3b} under different power levels

In particular, T_{30} reveals the whole state change of the system. In application, the parameter can be collected periodically during operation, and used as a reference. The difference between the collected T_{30} and the initial T_{30} should be considered as a translation in both T_3 and T_{3b}.

To prove the validity of T3 theory when applied to a stage change from a temperature influence, another experiment was carried out. The difference in

solenoid coil temperature was simulated by energizing the coil for different times from 0 to 8 min, under the same voltage and operating frequency. The mass discharge rate was then tested.
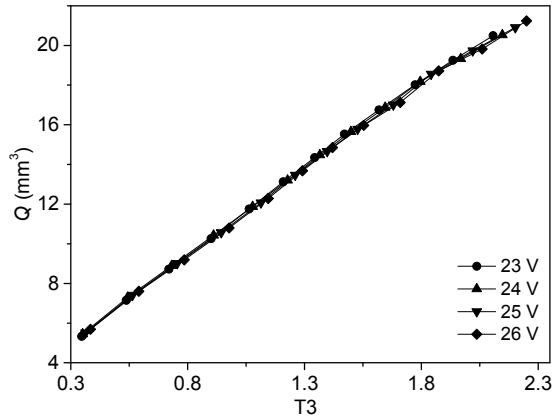
stalled on the exhaust pipe as a doser. DEF is supplied by a feeding pump to the doser then compressed, dosed, and injected with high pressure into the exhaust pipe.
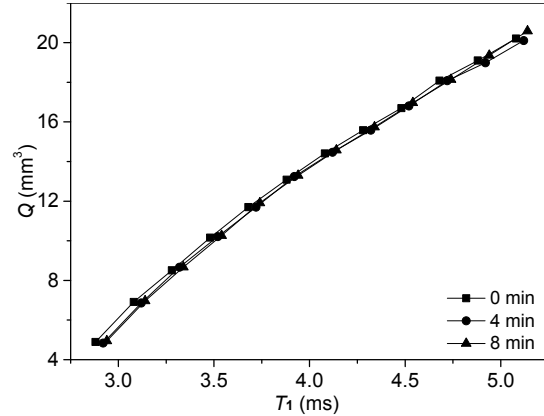

Fig. 9 Mass discharge against T3 at different power levels

Fig. 10 Mass discharge variation caused by changing temperature

The dispersion of mass discharge rate output under different coil temperatures was not large (Fig. 10), but the results were corrected to be almost negligible by the T3 model (Fig. 11).

The results shown in Fig. 9 and Fig. 11 indicate that parameter T3 is more precise in measuring the dosing rate.

5 Application of sleeve pump to DEF dosing systems

Air-assisted and airless DEF dosing systems, which are distinguished by whether compressed air is used to assist the liquid atomization, are the two systems widely used in diesel vehicles (Skovgaard and Babu, 2011). Both DEF dosing systems can be established using plunger-sleeve type dosing units.

A typical air-assisted dosing system is shown in Fig. 12. The sleeve pump type dosing unit is located on the bottom of the DEF tank as a submersible pump. The DEF is dosed by the dosing unit when compressed air is fed into the system, and the liquid/air mixture is dispensed through the mechanic nozzle.

Fig. 13 shows two sleeve pumps used for building an airless DEF dosing system. One is located on the bottom of the tank, but is used only as a feeding pump (not for DEF dosing), while the other is in-
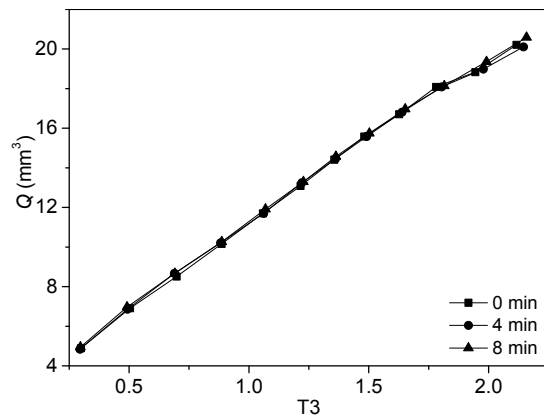

Fig. 11 Mass discharge results using T3 for different temperatures

Unlike the application to fuel injection systems for IC engine operation, DEF dosing does not require the same frequency as the operating engine, but an average dosing rate. Under the appropriate condition of the dosing rate range (mL/h or g/s), the dosing unit can keep the same mass discharge rate per cycle and adjust the dosing frequency to meet the dosing rate requirement for higher metering precision and less complicated control. Usually, the sleeve is driven to its maximum stroke, which is achieved by a limiting mechanism, and the maximum mass discharge volume in each cycle is dosed.
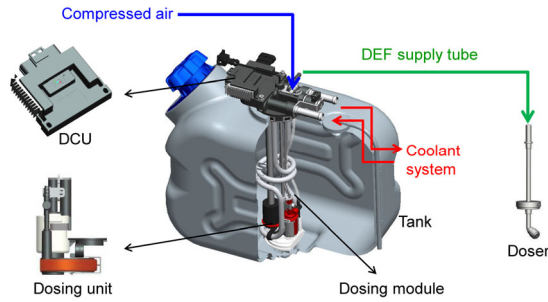
Fig. 12 Application of a sleeve pump type dosing unit to an air-assisted DEF dosing system
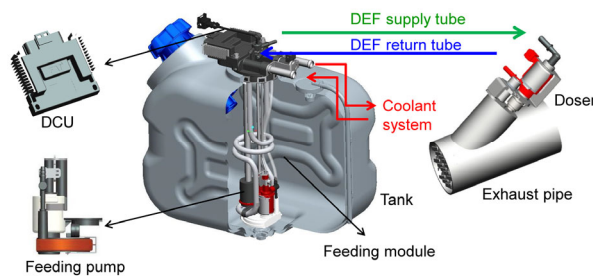

Fig. 13 Application of a sleeve pump type dosing unit to an airless DEF dosing system

6 Detection of failure modes using T_3

For a plunger-sleeve type dosing unit, several typical failure modes exist in dosing systems, as shown in Table 2.

Electrical failures can be easily detected by the control unit. Failure modes B and C can be detected with specific pressure sensors. However, a pressure sensor may not be the best choice. Furthermore, for sleeve type dosing units, some mechanical failures like a stuck plunger or a lack of liquid in chamber A cannot be detected by sensors. An emission deterioration test method usually delays detection and lacks clear identification of specific failure modes. Some

other flexible and reliable methods should be considered.

Failure modes B to D have similar features. All the faults, like the back pressure changing, blockage of the flow channel, sticking of the plunger-sleeve, or a lack of liquid, will greatly affect the mass discharge Q. According to the above T3 theory, this will greatly change T3 under the normal range of control pulse duration T_1.

Such a great change in T3 arises from both T_3 and T_{3b}, but mainly from T_3 because T_{3b} is pre-calibrated and responsible for only minor variation in practical applications. So these failure modes can be detected by the abnormally large variation in T_3. This means that the variation in parameter T_3 should be obvious and should be beyond the variation resulting from a state change such as power source voltage fluctuation or coil temperature variation when the failure occurs.

Typical dosing failure modes and their detection methods were examined in this study, including clogging and mechanical failure of pumping actions. Clogging usually occurs in the mixing chamber, DEF tube, or DEF nozzle. Mechanical failure is usually caused by a stuck plunger or a lack of liquid.

An experiment was carried out to investigate the effect of a blocked nozzle. The whole dosing system was built (Fig. 12). The source pressure was 0.8 MPa with a check valve in the air supply tube to prevent DEF back flow. A pressure sensor was used to measure the pressure in the mixing chamber. Both the pressure signal (P_m) and T_3 feedback were recorded. As the dosing unit was dosing at the rate of 1000 mL/h, the empty mixing chamber and the DEF pipe were gradually filled with DEF, and the pressure in the mixing chamber increased. Until P_m reached about 0.6 MPa, no obvious change in T_3 was observed. Then, with the increasing P_m due to the continuous

Table 2 Specific failure modes of air-assisted and airless dosing systems

Item	Type	Performance	Type of dosing system		Traditional detection method
			Air-assisted	Airless	
A	Electrical failures	Short circuit or break in line, coil or connector	Yes	Yes	By electrical circuit signal test with DCU
B	DEF tube or nozzle blockage	High pressure in the tube or nozzle	Yes	Yes	By pressure sensor
C	Short of compressed air	Low air pressure	Yes	No	By pressure sensor
D	Mechanical failures	Sleeve stuck, lack of liquid in chamber A	Yes	Yes	Emission deterioration test

discharge and the set of ball valve 2 upstream of the mixing chamber, the pressure in the chamber increased from about 0.6 MPa to about 2 MPa, and the feedback of T_3 apparently decreased from about 1.65 ms to 1.28 ms, which exceeded the normal T_3 range. The whole duration was about 18 s. The result revealed that a reasonable setting of the threshold of T_3 can detect the occurrence of clogging precisely and quickly. Moreover, the sudden changes in T_3 indicated by the arrows in Fig. 14 represented some active diagnoses executed by the DCU for the detection of mechanical problems.
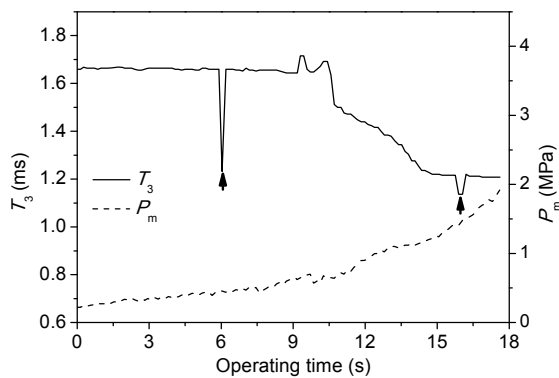

Fig. 14 T_3 data record when a nozzle is clogging

For failure due to mechanical problems, the normal operating T_3 cannot be used for detection directly. As discussed above, in normal operation cycles, the sleeve is driven to its maximum stroke. Under this condition, when the chamber A is empty, the variation in T_3 is too small to be used for failure detection, because it still intersects with normal T_3. This is caused by state change and that usually results in the possibility of error detection and high failure rates on the market. A substitution parameter of T_3 is used to solve this problem. After an invariable number of operation cycles, the DCU gives a shorter T_1 which pushes the sleeve to a shorter stroke. A much shorter T_3, called T_{3_EOBD}, is detected and has its own reasonable range. If the measured T_{3_EOBD} is outside the reasonable value range, mechanical failure caused by lack of liquid or a stuck plunger can be detected. Although a different DEF is dosed in the cycle for the T_{3_EOBD} test, the dosing frequency is adjusted in the following cycles before the next T_{3_EOBD} test to

compensate the discharge rate. Thus, the check period does not deteriorate the NO_x deduction efficiency.

Fig. 15 shows a T_{3_EOBD} test in a normal operating dosing system. The test is executed every 50 operating cycles. The feedback T_{3_EOBD} value is a little higher than the standard value, but is between the upper and lower values. Mechanical failures did not occur in the dosing unit. Once an abnormal value of T_{3_EOBD} was detected, a continuous mechanical failure test was executed for failure confirmation (Figs. 16 and 17). If the feedback T_{3_EOBD} remains larger than the upper limit or smaller than the lower limit value for a period of time, which can be set in logic, a mechanical failure is confirmed and the dosing unit will stop operation for self-protection.
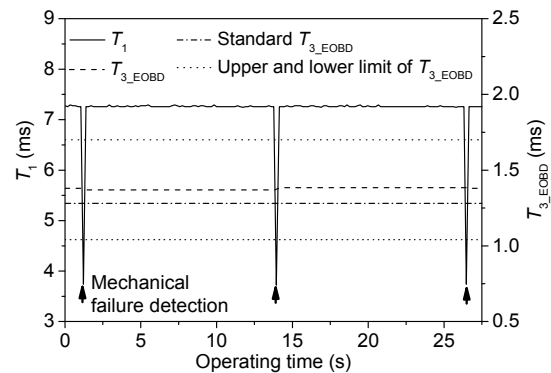

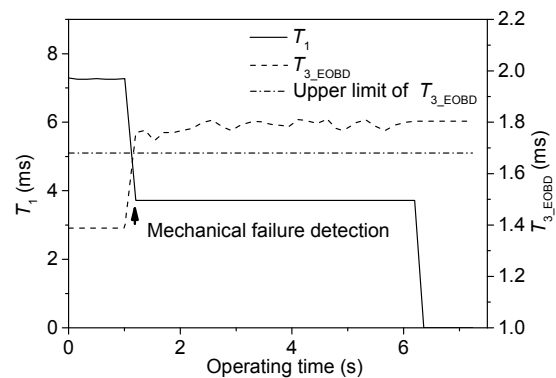**Fig. 15 T_{3_EOBD} test for mechanical failure detection**

Fig. 16 Mechanical failure caused by lack of liquid

The above analysis indicates the practicability of parameter T_3 for some kinds of failure detection in DEF dosing systems for SCR. More algorithms and logic should be added when used in products to avoid misjudgements.
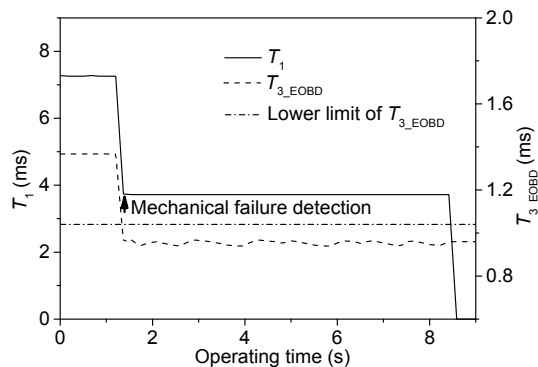
Fig. 17 Mechanical failure caused by a stuck plunger

7 Conclusions

In this paper, we describe a solenoid actuated plunger-sleeve type dosing unit for DEF dosing in SCR systems, along with its working process. The structure is simpler than that of other SCR DEF dosing pumps widely used in vehicles.

For solving the problem of metering precision of plunger-sleeve type dosing units under state changes in power level or temperature, a whole-state liquid measurement model is described, which connects the electrical energy with the mass discharge and a measurable variable, T3. By eliminating the effect of the state changes caused by temperature and power level, complex and difficult energy equations were reduced to a simple but stable model. In the model, the variables in the complicated process can be measured and solved with a highly efficient algorithm and the mass discharge can be controlled precisely in real-time.

In DEF dosing systems, the measurable time parameter T_3 can be flexibly used for typical failure mode detection. Tube clogging in air-assisted dosing systems and mechanical failure of pumping actions caused by lack of liquid or a stuck plunger were exemplified. Experiments were carried out to prove its validity and applicability. By connecting with reliable logic, the method can be widely used in products.

References

Biswas S, Verma V, Schauer JJ, et al., 2009. Chemical speciation of PM emissions from heavy-duty diesel vehicles equipped with diesel particulate filter (DPF) and selective catalytic reduction (SCR) retrofits. *Atmospheric Environment*, 43(11):1917-1925.
https://doi.org/10.1016/j.atmosenv.2008.12.040

Brandenberger S, Kröcher O, Tissler A, et al., 2010. The determination of the activities of different iron species in Fe-ZSM-5 for SCR of NO by NH₃. *Applied Catalysis B: Environmental*, 95(3-4):348-357.
https://doi.org/10.1016/j.apcatb.2010.01.013

Cloudt R, Willems F, van der Heijden P, 2009. Cost and fuel efficient SCR-only solution for post-2010 HD emission standards. *SAE International Journal of Fuels and Lubricants*, 2(1):399-406.
https://doi.org/10.4271/2009-01-0915

David BK, 1998. Engines and nanoparticles: a review. *Journal of Aerosol Science*, 29(5-6):575-588.
https://doi.org/10.1016/S0021-8502(97)10037-4

Fedeyko JM, Chen HY, Ballinger TH, et al., 2009. Development of Thermally Durable Cu/SCR Catalysts. SAE Technical Paper 2009-01-0899, SAE, USA.
https://doi.org/10.4271/2009-01-0899

Fitzgerald AE, Kingsley Jr C, Umans SD, 2003. Electric Machinery, 6th Edition. McGraw-Hill, New York, USA.

Grout S, Blaisot JB, Pajot K, et al., 2013. Experimental investigation on the injection of an urea–water solution in hot air stream for the SCR application: evaporation and spray/wall interaction. *Fuel*, 106:166-177.
https://doi.org/10.1016/j.fuel.2012.09.022

Hamada H, Haneda M, 2012. A review of selective catalytic reduction of nitrogen oxides with hydrogen and carbon monoxide. *Applied Catalysis A: General*, 421-422:1-13.
https://doi.org/10.1016/j.apcata.2012.02.005

Hayakawa K, 2007. Fuel Injection Control Method and Fuel Injection Control Device. US Patent 7273038.

Heeb NV, Zimmerli Y, Czerwinski J, et al., 2011. Reactive nitrogen compounds (RNCs) in exhaust of advanced PM-NO$_x$ abatement technologies for future diesel applications. *Atmospheric Environment*, 45(18):3203-3209.
https://doi.org/10.1016/j.atmosenv.2011.02.013

Heimberg W, Hellmich W, Kogl F, et al., 1996. Fuel Injection Device According to the Solid-state Energy Storage Principle for Internal Combustion Engines. US Patent 5520154.

Heywood JB, 1988. Internal Combustion Engine Fundamentals. McGraw Hill, New York, USA.

Kim JY, Richardson A, 1995. Study of Vapor Generation from Fuel System Components. SAE Technical Paper 952788, SAE, USA.
https://doi.org/10.4271/952788

Koebel M, Kleemann ME, 2000. Urea-SCR: a promising technique to reduce NO$_x$ emissions from automotive diesel engines. *Catalysis Today*, 59(3-4):335-345.
https://doi.org/10.1016/S0920-5861(00)00299-6

Lambert C, Hammerle R, McGill R, et al., 2004. Technical Advantages of Urea SCR for Light-duty and Heavy-duty Diesel Vehicle Applications. SAE Technical Paper 2004-01-1292, SAE, USA.

https://doi.org/10.4271/2004-01-1292

Lee P, Peterson A, Lai M, et al., 2010. Effects of B20 Fuel and Catalyst Entrance Section Length on the Performance of UREA SCR in a Light-duty Diesel Engine. SAE Technical Paper 2010-01-1173, SAE, USA.
https://doi.org/10.4271/2010-01-1173

Matthias B, 2015. Dosing Device. US Patent 0082775A1.

Moreno-Tost R, Oliveira MS, Eliche-Quesada D, et al., 2008. Evaluation of Cu-PPHs as active catalysts for the SCR process to control NO$_x$ emissions from heavy duty diesel vehicles. *Chemosphere*, 72(4):608-615.
https://doi.org/10.1016/j.chemosphere.2008.02.065

Needham D, Spadafora P, Schiffgens HJ, 2012. Delphi SCR dosing system–an alternative approach for close-coupled SCR catalyst systems. Proceedings of the 21st Aachen Colloquium Automobile and Engine Technology.

Oh J, Lee K, 2014. Spray characteristics of a urea solution injector and optimal mixer location to improve droplet uniformity and NO$_x$ conversion efficiency for selective catalytic reduction. *Fuel*, 119:90-97.
https://doi.org/10.1016/j.fuel.2013.11.032

Patel F, Patel S, 2012. Recent trends in catalyst development for diesel engine exhaust emission control. *Journal of Environmental Research and Development*, 6(4):1047-1054.

Scarnegie B, Miller W, Ballmert B, et al., 2003. Recent DPF/SCR Results Targeting US2007 and Euro 4/5 HD Emissions. SAE Technical Paper 2003-01-0774, SAE, USA.
https://doi.org/10.4271/2003-01-0774

Skovgaard M, Babu K, 2011. Application Experiences with Current Generations of SCR Dosing Systems in Euro 4, 5 and 6. SAE Technical Paper 2011-28-0027, SAE, USA.
https://doi.org/10.4271/2011-28-0027

Wang DY, Yao S, Shost M, et al., 2008. Ammonia Sensor for Closed-loop SCR Control. SAE Technical Paper 2008-01-0919, SAE, USA.
https://doi.org/10.4271/2008-01-0919

中文概要

题　目：用于选择性催化转化计量系统尿素溶液计量和故障诊断的 T3 计量模型

目　的： 一种新型的应用于选择性催化转化（SCR）尿素计量喷射系统的套筒式柱塞泵，其液体计量精度受环境状态（如驱动电压和温度等）变化的影响较大。通过对基于该套筒泵物理模型与驱动方式建立的能量方程与电学方程进行创新求解，得到一个与该套筒泵单循环的液体喷射量有稳定线性关系且对环境状态变化不敏感的参数 T3，以实现全状态计量精度控制。同时，利用 T3 模型中的 T_3 等测量参数，实现对基于该套筒泵建立的尿素喷射系统中部分典型故障的快速有效的车载（OBD）诊断。

创新点： 1. 通过 T3 液体计量模型可实现套筒式柱塞泵的液体计量精度控制；2. 通过 T3 模型中的 T_3 等可测量参数可对部分典型故障进行 OBD 诊断。

方　法： 1. 建立能量方程和电学方程，并通过无量纲化处理，推导出套筒式柱塞泵单循环液体喷射量与 T3 参数关系的全状态方程；2. 通过液体计量精度实验验证 T3 模型在环境状态变化时对液体计量精度控制的可靠性。

结　论： 1. 通过 T3 全状态模型，将电能与套筒泵单循环液体喷射量通过一个可测量的参数 T3 结合，可以实时进行喷射量反馈控制使套筒泵保持较高的喷射精度，且在环境变化（如电压或温度变化）时，仍能实现较高精度的控制。2. 实验证明，通过 T_3 等参数能对部分系统故障进行无传感器故障诊断，结合一定的控制逻辑可以满足 OBD 故障检测要求。

关键词： 尿素溶液计量单元；套筒式柱塞泵；T3 计量理论；无传感器诊断